Research Article Open Access

László Molnár*, Balázs Vásárhelyi, Tivadar M. Tóth, and Félix Schubert

Integrated petrographic – rock mechanic borecore study from the metamorphic basement of the Pannonian Basin, Hungary

Abstract: The integrated evaluation of borecores from the Mezősas-Furta fractured metamorphic hydrocarbon reservoir suggests significantly distinct microstructural and rock mechanical features within the analysed fault rock samples. The statistical evaluation of the clast geometries revealed the dominantly cataclastic nature of the samples. Damage zone of the fault can be characterised by an extremely brittle nature and low uniaxial compressive strength, coupled with a predominately coarse fault breccia composition. In contrast, the microstructural manner of the increasing deformation coupled with higher uniaxial compressive strength, strain-hardening nature and low brittleness indicate a transitional interval between the weakly fragmented damage zone and strongly grinded fault core. Moreover, these attributes suggest this unit is mechanically the strongest part of the fault zone. Gouge-rich cataclasites mark the core zone of the fault, with their widespread plastic nature and locally pseudo-ductile microstructure. Strain localization tends to be strongly linked with the existence of fault gouge ribbons. The fault zone with ~15 m total thickness can be defined as a significant migration pathway inside the fractured crystalline reservoir. Moreover, as a consequence of the distributed nature of the fault core, it may possibly have a key role in compartmentalisation of the local hydraulic system.

Keywords: fractured metamorphic reservoir; rock mechanical parameters; fault rocks; brittle deformation

DOI 10.1515/geo-2015-0004
Received March 25, 2014; accepted October 13, 2014

***Corresponding Author: László Molnár:** Department of Mineralogy, Geochemistry and Petrology, University of Szeged, Szeged, Hungary, Egyetem u. 2. H-6722, E-mail: molnar.laszlo@geo.u-szeged.hu

Balázs Vásárhelyi: Deptartment of Geotechnics and Engineering Geology, Budapest University of Technology and Economics, Budapest, Hungary

Tivadar M. Tóth, Félix Schubert: Department of Mineralogy, Geochemistry and Petrology, University of Szeged, Hungary

1 Introduction

Brittle fault zones of crystalline rock masses can serve as migration pathways or also as sealing surfaces for fluid flow in the Earth's crust, so the understanding of their internal structure is crucial for interpreting hydraulic systems. Earlier studies [1, 2] on the architecture of fault zones defined two main structural elements: first, a weakly disaggregated, densely fractured "damage zone" and a strongly deformed and fragmented "fault core", where the pre-existing rock fabrics were erased by fault development. These elements can be characterised by the formation of diverse tectonite types (fault breccias, cataclasites, fault gouges), which often also possess quite heterogeneous rheological features. Consequently, the petrological, petrophysical and rock mechanical properties may have an extremely heterogeneous spatial distribution in fault zones.

In addition, evaluation of tectonites from core samples always provide a serious challenge to proper structural interpretation, particularly due to the small number of borecores and their quite doubtful representativeness of the whole rock mass [3]. These constraints raise the necessity of integrated analytical methods that aim to gain as much information from these samples as possible.

The main aim of this paper was to present the results of one such petrographic, microstructure and rock mechanical analysis: we examined the lithological and rheological attributes of a basement fault zone with a quite high rate of core recovery and abundant amount of available samples, via the usage of these integrated methods. The combined petrographic (microstructural and clast geometric) and rock mechanical evaluations were conducted partly to clarify the role of main structural elements in the hydraulic system of both the fault zone and the whole fractured rock mass.

2 Geological setting

The locality of this study is the pre-Neogene basement of the Pannonian Basin (PB), which is part of Alpine-Carpathian-Dinaric orogenic belt, and which consists of deep sub-basins separated by subsurface topographic highs of metamorphic basement (e.g. [4, 5]). One of the best-known elevated basement highs is the Mezősas-Furta Dome (MFD), which is part of the series of metamorphic highs bordering the Békés Basin to the north (Fig. 1).

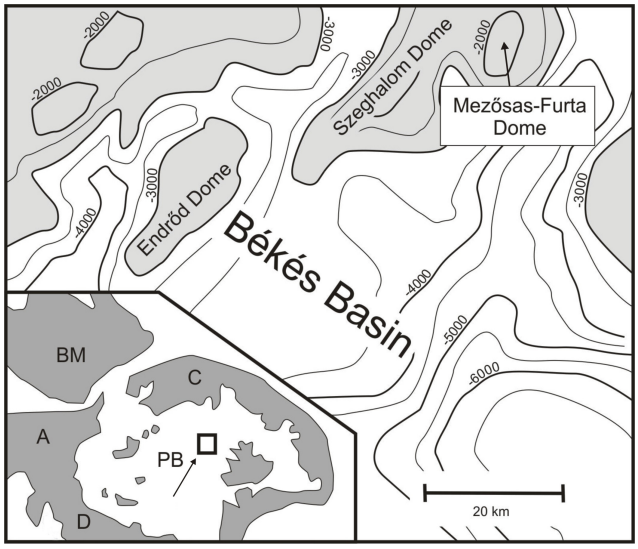

Figure 1: Topographic map of the Pre-Neogene basement of the eastern portion of the Pannonian Basin and the distribution of the basement highs (shaded). Isolines denote depth below the present surface in meters. Inset: Location of the studied well in the Alpine–Carpathian–Pannonian System. A – Alps, BM – Bohemian Massif, C – Carpathians, D – Dinarides, PB – Pannonian Basin.

Following the earliest studies on the area (e.g. [6] or [7]), detailed petrological investigations [8] defined the metamorphic evolution of the most typical lithologies of MFD and clarified their spatial arrangement through the basement high. The constructed idealized rock column suggests the presence three lithological blocks: at the uppermost structural level amphibolite and amphibole-biotite gneiss (AG group) with medium grade metamorphism is common. This group structurally overlays high metamorphic grade sillimanite and garnet bearing biotite gneiss that is often coupled with garnet-bearing amphibolite, and is jointly named the SG group. At the lowermost structural position orthogneiss is dominant, derived from medium-grade metamorphism of an igneous intrusion. The orthogneiss body is often cross-cut by microgranite dykes. These lithologies are jointly named the OG group. The rather different metamorphic evolutions of these groups and the presence of wide shear zones along the group boundaries indicate these blocks were juxtaposed following their metamorphic pressure-temperature peaks.

According to [8] in the central range of the dome the SG and AG units dominate on top of the basement, while the northern slope of the MFD is mainly built up by the OG unit. By the interpretation of these spatial data, the structure of the area can be explained as overthrusted NW-SE oriented stripes of AG/SG/OG triplexes. The simplified framework of the MFD can be described by parautochthonous OG unit with allochthonous AG/SG duplexes on the top. Details of microstructural investigations indicate that AG/SG boundary formed during an earlier compressional event and the two groups jointly overthrust the OG unit. These statements are in good agreement with the results of numerous authors [4, 9, 10], as the structure of the basement was strongly affected by Upper Cretaceous nappe formation, as well as sinistral transpression in the Middle Miocene period. This scenario was complicated on the southeastern portion of the MFD, where high-angle normal faulting related to the Neogene (Badenian) extension of the area formed horst-graben structures.

The multi-stage tectonic evolution of the area resulted in the presence of wide brittle fault zones throughout the crystalline highs, which also act as fractured hydrocarbon reservoirs in the basement of the PB, with the MFD reservoir being one example. By the inferences of [5], these fractured horizons, with their often-enhanced permeability, have a great impact on the hydraulic system of the metamorphic highs, and in fact these shear zones probably serve as the main migration pathways between the deep sedimentary basins and the fractured hard rock realm [5]. A wide fault zone was penetrated by a well (A-2) in the northern, OG-dominated part of MFD with a quite high core recovery (Fig. 2). The well is situated north of the hydrocarbon producing wells of the field in the most elevated parts of the metamorphic high (unpublished industrial data). Although, well A-2 itself is non-productive due to its structural position, the sampled fault zone may play a crucial role in the local petroleum system by linking the source rocks of the adjacent sedimentary sub-basins and the metamorphic high. In the absence of oriented borecores, high-resolution seismic sections or nearby wells, the kinematic sense and the spatial position of the approximately 10 meters wide fault zone are unclear. Nevertheless, the examined section that consists of diverse fault rock samples give an outstanding opportunity for an integrated evaluation of the shear zone.

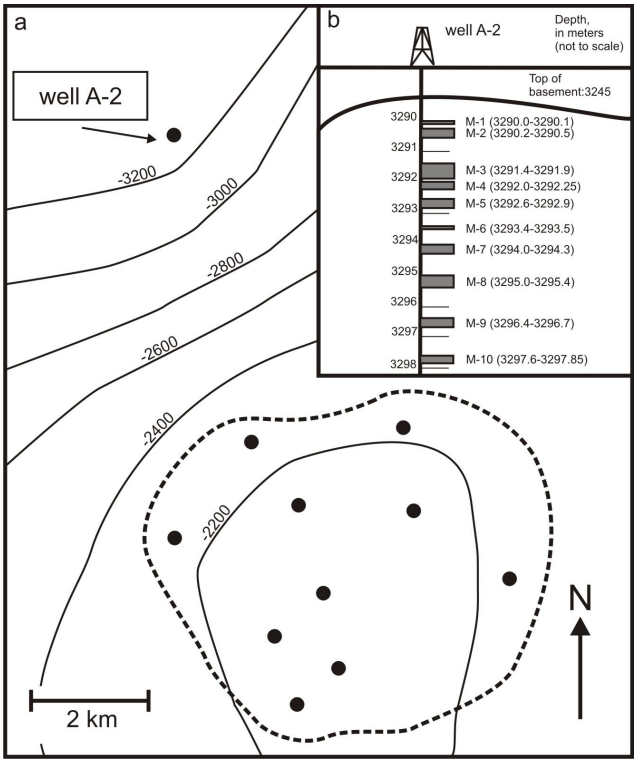

Figure 2: a: Detailed sub-surface topography of Mezősas-Furta Dome. Dots mark the productive wells of the field, while the dashed line indicates the assumed location of the main hydrocarbon accumulation. Isolines denote depth below the present surface in meters. b: Schematic vertical section of the investigated well and borecores evaluated in this study. The grey rectangles indicate the location of the samples.

3 Samples and applied methods

3.1 Available samples

All 10 available borecores from well A-2 were sampled in the depth interval between 3290 and 3297.85 meters below sea level with high core recovery (detailed in Fig. 2/b). All of the rock specimens were affected by various degrees of brittle deformation. The cores were not oriented. For Petrographic Image Analysis of the fault rocks, 78-414 clasts were measured from each sample.

3.2 Petrographical and microstructural observations

Following the preliminary macroscopic analysis, thin sections were evaluated from all 10 borecores for the petrographic investigations to define the microstructural characteristics of the diverse fault rock types. The available thin sections were made perpendicular to the foliation and parallel to lineation.

3.3 Description of Petrographic Image Analysis (PIA)

The PIA of samples was conducted with the aim of defining the geometric features of clasts within the fault rocks. First, polished surfaces were cut parallel to the longitudinal axis of the borecores, then 2D images were taken (Fig. 3). Unfortunately, as some of the available thin sections did not provide a statistically sufficient amount of observable particles (>50 clasts), the micro-scale samples were omitted from the image analysis. The lower limit of the image analysis was 100 pixel^2 (0.16 mm^2), according to the suggestions of [11, 12] on the methods of particle size/shape analysis, while the size of the largest measured clast was 193960 pixel^2 (293 mm^2). However, in this case the clasts could not be segmented by the use of a colour threshold application as the matrix or cement was too heterogeneous, so the selection of edges was accomplished manually, using the "Magnetic Lasso" tool of Adobe Photoshop. The clast geometric measurements were completed using the selected parameters in ImageJ. The applied parameters are discussed below.

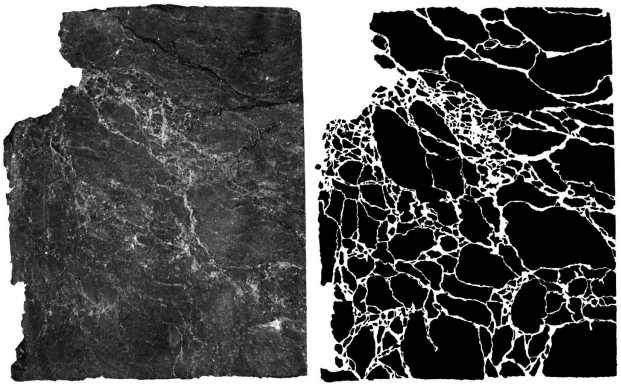

Figure 3: Polished surface of a borecore from well A-2 (sample M1) and the clasts selected for measurements, drawn one-by-one in Adobe Photoshop. The diameter of the borecore is 6.5 centimeters.

3.3.1 Particle Size Distribution (PSD)

Earlier studies [13–15] demonstrated the fractal nature of the cumulative *PSD* of the fault rocks, with the following

Table 1: Published grain size distribution data of brittle fault rocks, based on the results of [13–16].

Authors, year	*Rock type*	*Natural/experimental deformation*	*2D fractal dimension*
Sammis et al., 1987	Granite	Natural	1.6
Blenkinsop, 1991	Granite, gneiss	Natural	0.8-2.1
Blenkinsop, 1991	Arkose	Natural	1.6-2.0
Storti et al., 2003	Carbonates	Natural	0.9-2.5
Keulen et al., 2007	Granitoids	Natural	1.6-2.4
Keulen et al., 2007	Granitoids	Experimental	1.4-2.3
This study	Gneiss	Natural	1.12-1.72

equation: $N(s) \sim s^{-Ds}$. The $N(s)$ is the number of particles smaller than a size s (square root of the area), while D^S can be determined as the slope of the best fit line on a log $N(s)$ against log$s$ graph. Different D^S values are expected for varying degrees of the fragmentation process and different tectonic settings or rock types, according to the data of [14–17] (Table 1).

3.3.2 Clast complexity (D^R)

Based on the results of [11], "Fractal Dilation" is the most precise method for the determination of clast complexity. The "Fractal Dilation" macro of ImageJ uses a 1 pixel-wide outline of the clasts, which are thickened, creating 2, 4, 8 and 16 pixel-width ribbons. The area of these ribbons is plotted against its thickness on log-log plot, where the slope of the best fit line (S) is the indicator of clast-complexity fractal dimension (D^R) using the $2\text{-}S = D^R$ equation.

3.3.3 Aspect Ratio (AR)

The Aspect Ratio (AR) is the proportion of the long and short axes of the ellipse that best fits the outline of a clast. The ellipse has the same area, long-axis orientation and centre as the original grain, defined by ImageJ.

3.3.4 Circularity (Circ)

The value of circularity can be expressed by the equation of $4\pi(AP/p^2)$, where AP is the area of the clast, and p is its perimeter [18]. This measures how close the particle's shape is to a perfect circle. According to the above formula, the value of the *Circ* varies between 0 and 1, where 0 is an immensely elongated ellipse, while 1 is a perfect circle.

3.3.5 Orientation Angle (Angle)

The numerical value of orientation for a single clast is the angle between the long-axis of the clast's best-fit ellipse and the lateral (the "X") axis of the image. The best-fit ellipse and the long-axis angle are both computed by ImageJ. The degree of orientation is observable in the dispersion from the average *Angle* values of the clasts, which is numerically manifested in the changes of relative standard deviation values.

3.3.6 Convexity (Conv)

Convexity measures the surface roughness of a particle, calculated by dividing the convex hull perimeter by the actual particle perimeter, so the smooth shapes have a *Conv* value close to 1, while the spiky and irregular objects have a *Conv* value closer to 0.

3.3.7 Statistical analysis of the fault rocks

The brittle fault rock samples were classified by multivariate statistical analysis of their clast geometric parameters (Table 2/a). The method (detailed in [19]) was developed and tested on the fault rocks of the nearby Szeghalom basement high, which have a quite similar lithological composition as MFD [5]. In this approach, statistically sufficient amounts of samples (~3000 clasts) were measured with the same PIA procedure and their datasets were analysed via multivariate statistical methods. Separation of the three main fault rock types were achieved without any overlap [19] by using two calculated discriminant functions (D1, D2) [20, 21]. The calculated discriminant functions were the following, with the weights of the most important parameters:

$$D1 = 0.731 * PSD - 0.588 * Angle + 0.553 * Circ \quad (1)$$

$$D2 = 0.974 * AR + 0.94 * PSD - 0.271 * Circ \quad (2)$$

Table 2: Measured clast-geometric data (a) and mechanical constants (b) of the investigated samples.

a

Sample	Depth [m]	*PSD*	D^R	*AR*	*Circ*	*Conv*	*Angle*
M1	3290.00-.10	1.18	1.32	1.59	0.72	0.91	0.63
M2	3291.20-.50	1.12	1.19	1.51	0.75	0.92	0.74
M3	3291.40-.90	1.27	1.44	1.79	0.71	0.9	0.64
M4	3292.00-.25	1.37	1.36	1.87	0.64	0.87	0.61
M5	3292.60-.90	1.14	1.41	2.19	0.65	0.86	0.45
M6	3293.40-.50	1.41	1.39	1.89	0.67	0.89	0.62
M7	3294.00-.30	1.52	1.45	2.07	0.63	0.88	0.51
M8	3295.00-.40	1.63	1.48	1.88	0.66	0.87	0.55
M9	3296.40-.70	1.45	1.37	2.18	0.68	0.88	0.42
M10	3297.60-.85	1.72	1.41	1.87	0.61	0.85	0.53

b

Sample	Depth	σ_c	σ_{cd}	Young modulus	Poisson rate	E / σ_c	σ_{cd} / σ_c	Wt	We	B=We/Wt
	[m]	[MPa]	[MPa]	[GPa]	[-]		[%]	[kJ]	[kJ]	
M1	3290.00-.10	13.78	12.34	6.7	0.13	486	89.6	19.06	14.17	0.74
M2	3291.20-.50	21.08	16.54	10.22	0.21	485	78.5	26.86	21.74	0.81
M3	3291.40-.90	17.63	16.77	7.85	0.1	445	95.1	21.71	19.8	0.91
M4	3292.00-.25	25.33	19.23	8.98	0.37	206	75.9	188.57	35.72	0.19
M5	3292.60-.90	31.9	28.32	11.19	0.38	351	88.8	108.87	45.47	0.42
M6	3293.40-.50	22.37	19.21	11.01	0.33	492	85.9	90.34	22.73	0.25
M7	3294.00-.30	15.32	14.29	8.25	0.15	586	93.3	26.78	14.22	0.53
M8	3295.00-.40	26.99	18.68	14.52	0.14	538	69.2	50.18	25.08	0.5
M9	3296.40-.70	10.88	9.02	5.85	0.16	538	82.9	18.88	10.12	0.54
M10	3297.60-.85	19.61	17.18	8.23	0.19	361	87.6	43.46	23.36	0.54

3.4 Rock mechanical tests

In accordance with the suggestions of the International Society for Rock Mechanics [22] regular cylindrical shapes were created with the standard 2:1 (axis:diameter) size and 50 mm diameter. Only one sample was cut from each borecore due to their limited size. Rock mechanical tests were carried out in the Rock Mechanics Laboratory at the Budapest University of Technology and Economics.

Uniaxial compressive tests, widely used for defining rock mechanical properties, were applied to study the mechanical properties of the study samples. If the lateral surface of the sample is traction-free, the experimental configuration can be characterised by the $\sigma_1 > 0$, $\sigma_2 = \sigma_3 = 0$ equation. Accepting these statements, the uniaxial compressive strength (σ_c) (MPa) of the samples is derived from the measured uniaxial strain (ε) and uniaxial stress (σ) values. The plot of σ against ε defines the stress-strain curve, where the maximum stress value is the uniaxial compressive strength (σ_c) (MPa). The Young or elastic modulus (E) (GPa) of the samples can be experimentally determined from the slope of the stress-strain curve at 50% of the ultimate stress, by the advice of [22]. The Poisson's rate value (ν) is the ratio of the axial and lateral strains at this point.

Several characteristic stress levels can be determined through laboratory tests that are essential for understanding the failure (damage) process of brittle rocks during compression:

- σ_{cc} is the crack closure stress level,
- σ_{ci} is the crack initiation stress level,
- σ_{cd} is called the crack propagation stress level. This latter parameter is close to the longterm rock strength [23, 24].

The above three stress levels, i.e., σ_{cc}, σ_{ci}, and σ_{cd}, show important stages in the macroscopic damage process of intact rocks. Crack initiation starts at stress levels of about 1/3 to 2/3 times the peak uniaxial load (σ_f) for most brittle rocks [25, 26]. The crack propagation stress level (σ_{cd}) is the stress level at which the maximum total volumetric strain is attained, which can be calculated from the stress-volumetric strain curve [26].

According to [27], the coefficient of brittleness can be calculated as the ratio between the elastic work (W_e) and the total or destruction work (W_t) during the loading of a specimen until failure. Destruction work (W_t) can be calculated from the measured stress-strain curves, as it is defined by the area under the measured stress-strain curve and reveals the amount of energy necessary for the failure of the sample. The elastic work (W_e) is also derived from the measured stress-strain curve, but is instead the amount of necessary energy in its elastic stage. The brittleness of samples (B) is the ratio of the elastic and destruction work values ($B = W_e/W_t$).

4 Results

4.1 Petrographical and microstructural observations

The fault zone of A-2 is mainly composed of cataclasites (Fig. 4/a), according to microstructural properties of the samples. However, locally other fault rock types are also observable: a coarse breccia without any preferred orientation and the sporadic fault-gouge ribbons occur, which cross-cut the cataclasites.

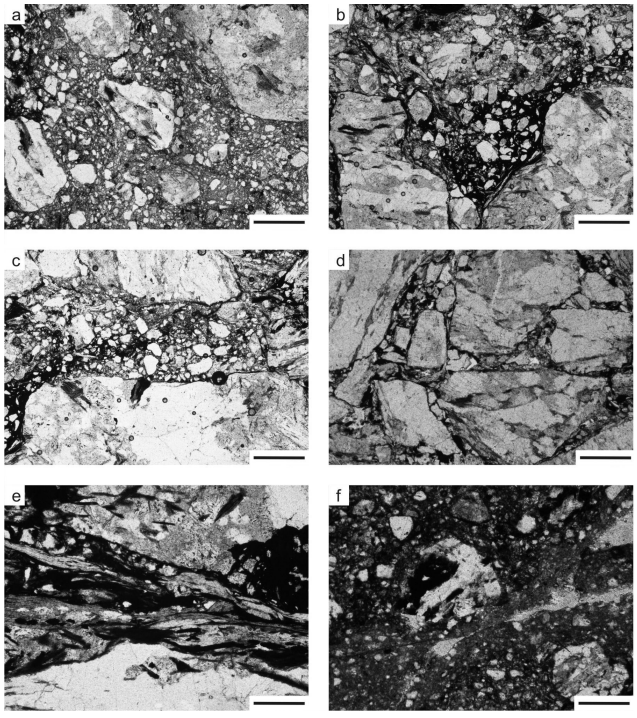

Figure 4: Photomicrographs representing characteristic fault rock textures from the samples from well A-2. a: Typical cataclastic texture, which is the most frequent structure of the samples with fragmented and rotated particles (sample M5). b: Strongly deformed domains between the centimeter-scale particles (sample M6). c: Planes of intensified deformation denoted by strongly fragmented cataclastic texture among relatively less deformed coarse grains (sample M4). d: Dilational domain with a weakly disaggregated texture, indicating a characteristic fault breccia texture (sample M2). e: Strongly foliated fault gouge plane with restricted distribution. The foliation is defined by the phyllosilicate flakes (sample M8). f: Granular fault gouge, which is regarded as the location of the largest fault displacement. Note the extremely high matrix ratio, which indicates the comminution of the clasts (sample M10). The scale bars are 500 μm long.

The internal structure of the cataclasites shows a strongly disaggregated appearance with angular clast geometry, even though macroscopically the external cohesiveness of the cataclasites is more or less remained. The grain size is dominantly under millimeter-scale and the ratio of particles over 2 mm is under 30%, the limit between the breccia/cataclasite series (Fig. 4/b,c). Samples often have a strong microscopic grain-shape orientation (GSPO) [28]: clasts are elongated and their long-axes define the preferred direction. This direction of the GSPO is generally subparallel to the supposed main shear direction. The phenomenon is usually coupled with the manner of cataclastic deformation, namely intensive clast-rotation, comminution and pervasive microfracture propagation (Fig. 4/c). The particles have a recognizable gneissic precursor with a quartz-feldspar-biotite dominated composition, which is derived from the undeformed wall rock of the OG group. The clasts of cataclasites did not suffer significant chemical alteration, only the largest particles have sporadic clay coating on their edges. The intense deformation often manifests in an anastomising, flow-banded structure with the local appearance of the S-C structures, indicating a semi-brittle style deformation.

The rather subordinate fault breccia samples mainly consist of coarse grained, angular clasts (often over centimeter-scale) (Fig. 4/d). The coarse breccia structures are locally prevalent in the samples M1, 2, 3. These samples typically have a chaotic texture often without any structural manner of preferred orientation. The largest clasts often can be fitted along their sharp, dilational edges indicating their mosaic, "jigsaw" type structure [18]. The gneissic origin of the fault breccia clasts is also recognizable.

In a few cases, the cohesive cataclastic texture is cross-cut by thin, clay-rich layers of incohesive fault gouge, especially in samples M -5, -7, -8 and -10. According to the microscopic investigations, the fault gouge ribbons have a very low clast/matrix ratio, indicating their strongly deformed nature, which is strengthened by the totally fragmented architecture of the clasts (Fig. 4/e,f). The protolith of the fault gouges is not recognizable, as their particles are mainly composed of mono-crystalline quartz. The comminuted clasts are always embedded in strongly altered clay-rich matrix. Appearance of these planes is restricted to millimeter wide anastomising planes with a sharp boundary towards the relatively less deformed cataclasites.

4.2 Clast geometric results

The clast geometric results with their mode values are summarized in the Table 2/a. Exceptions are the *PSD* and the *Angle* values, as the *PSD* was calculated from the slope of the grain size curve's best-fit line, while the *Angle* value

represents the variation coefficient of the particle's long axis direction in the actual sample.

Elongation of the clasts (*AR*) of the least deformed, brecciated samples is about 1.5 – 1.8, while in the cataclasites slightly higher numbers are typical (∼1.9). The highest *AR* values are observable in the most deformed or gouge-bearing cataclasites, where elongation ratios over 2.0 are frequent, especially in samples M5 and M9. Measurements of clast circularity (*Circ*) resulted in a slightly decreasing trend from the 0.7 values of less deformed borecores (with M2 as a maximum: 0.75) to ∼0.6 values in gouge-containing samples (with M10 as minimum: 0.61). Fractal dimensions of particle size distributions (*PSD*) reflect a gradual but constant increase towards the more fragmented samples: the lowest value is in the M2 with 1.12 cumulative *PSD* dimension, and the highest is in M10 with 1.72. In contrast, the numerical manifestation of the clast orientation, the relative standard deviation of the long axis directions is strongly decreasing in harmony with the observed intensifying microstructural deformation. The maximum value was calculated for the M2 (0.74), while the minimum is in the M9 (0.42). The clast complexity values reflect rising dimension with observed deformation from the 1.19 D^R values of M2 to the 1.48 of M8, while the convexity values are generally around 0.85 – 0.9, with a lack of any tendency.

4.3 Rock mechanical tests

The results of the uniaxial compressive tests and their derived data are summarized in the Table 2/b.

In Figure 5/a, the uniaxial compressive strength results (σ_c) were plotted against the crack propagation stress levels (σ_{cd}). Our results (83%) are in harmony with literature data [22], which define the onset of crack propagation at ∼85% of the uniaxial compressive strength. The Young or elastic modulus (E) values reflect a good correlation with uniaxial compressive strength results (σ_c) (R^2 =0.93) (Fig. 5/b), however, samples M4 and M5 were omitted from this plot, due to their strongly characteristic stress-strain curves. From the aspect of the destruction work (W_t), samples M4, M5 and M6 have an outstanding high necessary energy amount under the stress-strain curves (90.34 – 188.57 kJ) in contrast with other samples, where 50.18 kJ was the maximum value (M8) (Table 2/b).

The uniaxial compressive test results (σ_c) can be divided into three different stages according to the depth of the samples (Fig. 5/c). Down to 3291.9 meters in depth the borecores display a quite brittle nature with a very low uniaxial compressive strength (σ_c). Down to 3294 meters the stress-strain curves indicate extremely wide ductile and locally strain-hardening stages before their failure. The gradual transition from the rigid upper part towards the relatively ductile depth intervals is observable in samples M4, M5 and M6 with a ∼10 MPa higher uniaxial compressive strength (σ_c) than the borecores from shallower depth and the appearance of plasticity or even significant strain-hardening.

A similar process is observable in the calculated brittleness (B) data of the samples, which is the ratio of the elastic work (W_e) and the destruction work (W_t) (Table 2/b and Fig. 5/d). Borecores M1, M2 and M3 have a high B value close to 1 (B=0.743-0.912), while samples below 3294 meter depth can be characterised with lower B values (0.500 – 0.538). In the case of samples M4, M5 and M6 extremely low B ratios (between 0.189 and 0.418) were calculated.

5 Discussion

5.1 Interpretation of the microstructural data

The presence of the strongly fragmented cataclasites indicates that the whole analysed section was affected by a relatively strong deformation (Fig. 4). In this sense, samples M1, -2 and -3, with their local fault breccia structures can be interpreted as evidence for locally weaker disaggregation compared to the dominant fault rocks. On the other hand, the sporadic fault gouge ribbons are indicative of the most intense deformational stage of the whole rock mass [29], despite these planes always having a subordinate occurrence, even in micro-scale (Fig. 4/e,f). This arrangement can possibly be explained by the appearance of the strain localization [29], which concentrates the progressive deformation into thin layers of clay-rich gouges via a positive feedback process, similarly as the deformation bands develop in porous rocks [30, 31].

During the statistical examination of the Furta tectonites, their PIA data were plotted on the graph D1-D2 discriminant functions and illustrated together with the reference data in Fig. 6. As shown, most of the analysed samples are in the cataclasite category, in agreement with the microstructural observations. During the petrographic interpretation three samples displayed mixed fault breccia - cataclasite structures (M1, 2 and 3) and according to the discriminant analysis, two of them (M1 and M2) reflect a dominantly fault breccia-like clast geometry. In contrast, sample M3 was statistically classified as a cataclasite.

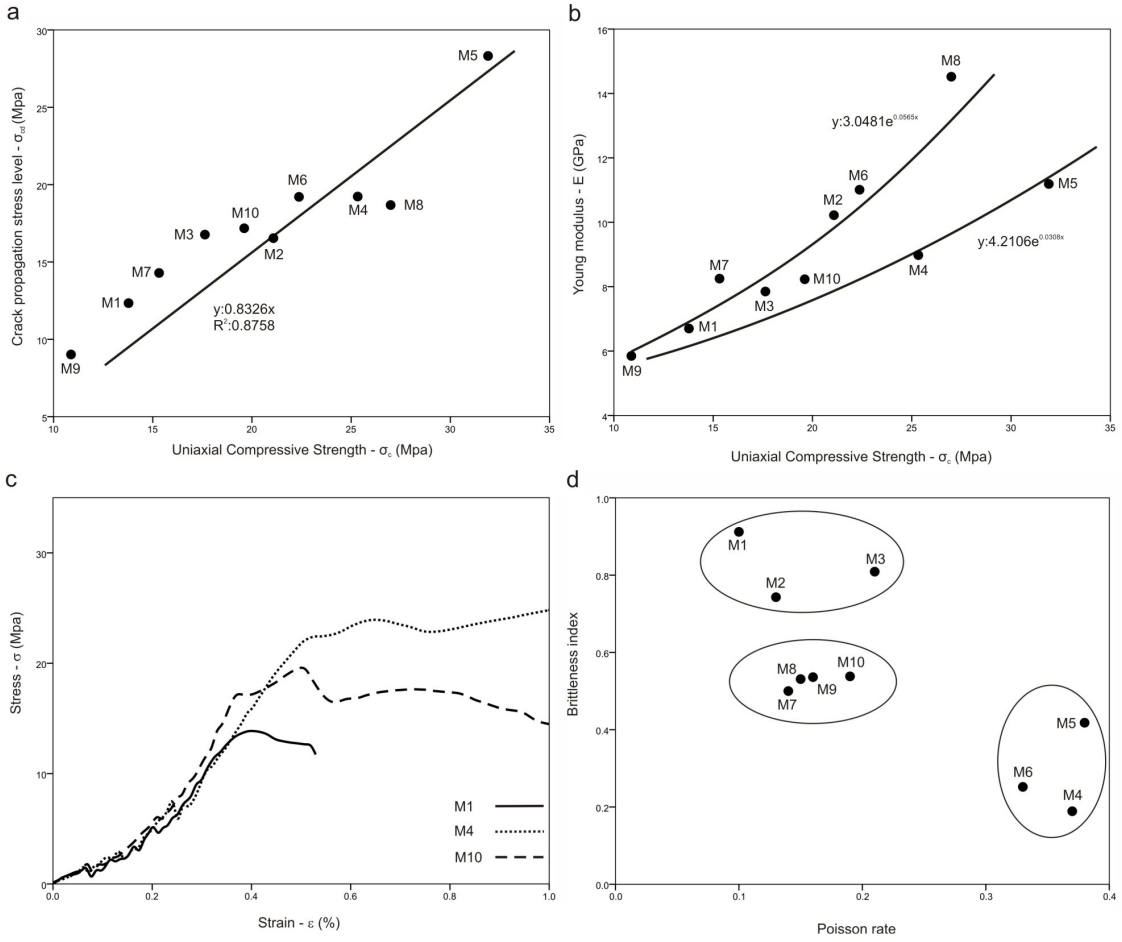

Figure 5: a: Illustrated plot of the uniaxial compressive strength and crack propagation stress level, which defined the onset of stable fracture growth at 83% of the longterm rock strength, which generally agree with the 85% value of the general [22] suggestions. b: Plot of uniaxial compressive strength and Young modulus reveals a quite strong increasing trend of the measured rock mechanical features, while only two of the samples (M4 and M5) do not fit to this trend. c: The characteristic stress-stain curves from A-2. Sample M1 a strongly rigid nature with low uniaxial compressive strength. M4 represents relatively higher σ_c and necessary work for the failure of the sample, indicating a strain-hardening nature. In contrast, the stress-strain curve of M10 reveals its strongly plastic and inelastic nature. These rock-mechanical features follow each other with increasing depth. d: Plot of measured Poisson rates versus the brittleness indices with the quite clear separation of the samples derived from distinct fault components: the damage zone (M1-3), the transition zone (M4-6) and the fault core (M7-10).

It is notable that none of the samples fall into the fault gouge category. This outcome possibly relates to their limited appearance and to the previously mentioned very low clast/matrix ratio compared to the adjacent cataclasites. As a consequence, this inevitably leads to the statistical underrepresentation of these domains, even in the most fault gouge dominated samples (e.g. M8 or M10).

In the light of these microstructural inferences and the possible arrangement of the fault rocks, the weaker disaggregated breccias presumably mark the fragmented damage zone component of the fault based on the interpretation of [1] or [32]. In contrast, the cataclasites often crosscut by gouge surfaces must relate to the fault core, which is the scene of the most considerable displacements [33]. The representative grain size distribution diagrams from the three main petrographic zones clearly illustrate the increasing *PSD* values with the observed increasing deformation (Fig. 7): this process is visible in the decreasing amount of relatively larger particles (i.e. over the 2 mm limit) in agreement with the observations of [15] or [17]. Consequently, relatively lower *PSD* dimensions of the breccia dominated samples (<1.3) also indicate that this part of the fault zone can be defined as the damage zone, according to the results of [16]. In contrast, the most deformed gouge-rich samples exceed the theoretical 1.6 *PSD* value of the gouge formation as it was described by [14, 17]. According to their evaluations on both naturally and experimentally deformed fault rocks the onset of fault gouge forma-

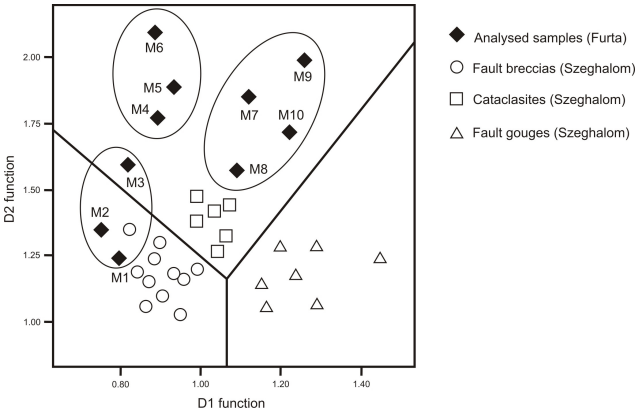

Figure 6: Illustration of measured fault rock samples from well A-2 based on their calculated D1 – D2 values (detailed in [19]) with characteristic values for each fault component. The reference data of the classification derived from the adjacent Szeghalom Dome are also displayed.

tion is always coupled with the process of shear localization and so, the further particle comminution.

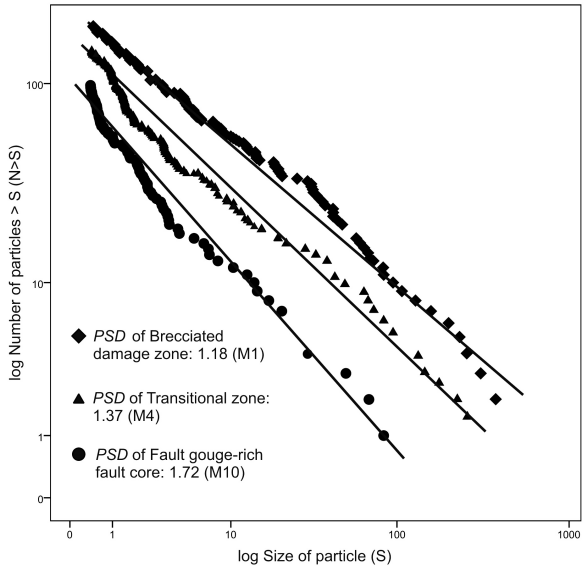

Figure 7: Characteristic grain size distributions from the three main petrographic zones. These domains reflect higher *PSD* values with the stronger observed deformation. The coarse grained brecciated samples have relatively lower *PSD* dimensions (<1.3), while, following the transitional values of the cataclasites, samples from the fault gouge-rich zones have the highest PSD dimensions (>1.6). This latter group can be characterised with increasing comminution and particle size reduction with intensive gouge formation and strain localization.

5.2 Rock mechanical properties of the fault rocks

The complex structure of the fault zone in well A-2 is also visible in light of the uniaxial compressive test results. The petrographically defined fault breccia nature of M1 and M2 samples can explain their low uniaxial compressive strength and brittle behaviour (Table 2/b and Fig. 5/a). Moreover this tendency possibly continues in the sample M3, despite that it was characterised as cataclasite. Their quite rigid nature possibly relates to the dominantly stick-slip style frictional sliding as a typical feature of the coarse grained, "immature" fault rocks [33].

The stress-strain curves of samples M4, M5 and M6 (Fig. 5/c) strongly deviate from this trend with their strongly inelastic nature and higher uniaxial compressive strength (Table 2/b and Fig. 5/a). This phenomenon presumably relates to the formation of the clay-rich fault gouge ribbons in this depth interval, which tend to accumulate the displacement through a stable sliding style motion coupled with strain localization in these zones, as is characteristic of the "mature" fault rocks [33]. Additionally, the remaining cohesiveness may be responsible for the observed strain hardening processes in these samples, as inferred by the relatively high destruction work (W_t) required for failure during testing.

Samples M7-10 display an extremely strong ductile and inelastic nature, without any observable trends in rock mechanical parameters with increasing depth (Table 2/b and Fig. 5/a). The extremely wide plastic stage on the stress-strain curves (Fig. 5/c) is a reflection of the fault gouge appearance and strain localization, even in a more dominant form than in the previous samples. In addition, the lower destruction work (W_t) values compared to M4, M5 and M6, imply that the strain-hardening is a less important process at these depth intervals. These data tend to emphasize that, though gouge surfaces microstructurally have only a secondary relevance, their spatial density presumably controls the rock mechanical properties of the fault rocks, which manifest in the formation of strong plasticity and weak elasticity in the most mature fault rock samples.

The plot of the Poisson ratio versus the calculated brittleness values (B) also indicate the quite clear separation of the petrographically defined units based on their rock mechanical features (Fig. 5/d). On the other hand, this strong correlation between uniaxial test results points out the validity of the microstructural classification as well.

5.3 Architecture of the A-2 fault zone

According to the integrated petrographical and rock mechanical investigations, three characteristic zones can be separated along the analyzed section of well A-2 (Fig. 8):

- Brecciated damage zone (M1-3)
- Transition zone (M4-6)
- Fault gouge-rich fault core zone (M7-10)

The uppermost zone – which was described as the damage zone of the fault – can be characterised by an extremely brittle nature and low uniaxial compressive strength, coupled with a dominantly coarse fault breccia composition. The microstructural characteristics of the increasing deformation in samples of M4-6, coupled with higher uniaxial compressive strength, strain-hardening nature and low brittleness indicate the semi-brittle features of the suspected border between the weakly fragmented damage zone and strongly ground fault core. Moreover, these attributes suggest this transitional interval is the mechanically strongest part of the fault zone. From the sample M7 downwards, gouge-rich cataclasites mark the core zone of the fault, with their widespread plastic nature and locally pseudo-ductile microstructure. As a consequence, this lowermost zone is presumably an indicator of main slip zones, where most of the displacement accumulated. Generally, the strain localization tends to be strongly linked with the existence of fault gouge ribbons in crystalline rocks (Fig. 4/e,f), as implied by the results of [2, 34].

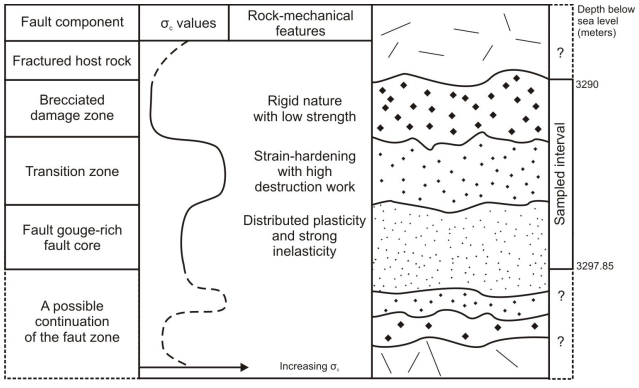

Figure 8: Schematic composition of the fault zone according to the integrated results of the petrographic and rock-mechanical investigations. For each fault components, their most characteristic features are displayed with the σ_c data. Increasing σ_c data towards the undeformed wall rock is presumed due to their less deformed nature. Literature data on the architecture of brittle fault zones suggest the downward continuation of the deformed horizons. Thicknesses of the fault units are not to scale.

The structure of the fault zone further down in depth intervals without borecores – regarding its width and distribution – can only be estimated with a limited reliability, due to the low number of the available samples. However, based on the theoretical fault zone architecture defined by earlier works [1, 2, 16], the deformed intervals has to continue downward toward the undeformed footwall with a symmetric geometry and a fault zone with ~15 meters of overall vertical thickness is possible (Fig. 8). This fault width can be compared with the observed major basement shear zones in the adjacent Szeghalom [5] and - similarly - can be interpreted as a main structural element of MFD [8].

The analyzed fault zones in the nearby Szeghalom basement high include distributed damage zones and play a crucial role in the hydrodynamics of the crystalline mass, especially in fluid migration. According to the unpublished industrial data from the Szeghalom reservoir, economic amounts of hydrocarbons were produced from these strongly brecciated intervals and the adjacent fractured wall-rock. This observation indicates that a shear zone with rather similar internal structure and geometry of the A-2 well could also be associated with significant porosity and permeability enhancement. Although the fault zone of A-2 is quite far from the main petroleum accumulation in the MFD reservoir (Fig. 2), its shear zone can serve as an essential conduit zone of the local hydrocarbon system. On the basis of the most likely scenario [5], hydrocarbons could migrate from the adjacent sedimentary sub-basins into the fracture network of the metamorphic high through the intensely brecciated damage zones of these wide fault zones.

It is known from the Furta field that the 12 productive wells produce at least 7 hydrocarbon fluids that are all different chemically (unpublished report) and these observations indicate that the fractured hard rock reservoir is highly compartmentalized hydrodynamically. From this point of view, the thicknesses of the damage zone and the fault core along the migration pathways are of key importance. The weakly disaggregated damage zone presumably tends to form a connected fracture network with relatively elevated permeability compared both to the undeformed wall rock and the fault core. On the other hand, due to its clay-rich, ductile and thus impermeable behaviour, the core could contribute to the hydrodynamically compartmentalized behaviour of the whole fractured mass [1, 34, 35].

6 Conclusion

The well A-2, in the Mezősas-Furta Dome (MFD) provided a large number of borecores with different degrees of deformation. On the basis of an integrated investigation, the petrologically defined fault units have remarkably different rock mechanical behaviours. We suggest that brecciated damage zone may have the best reservoir characteristics, due to their weakly disaggregated structure coupled with quite rigid rheological features. In contrast, the transition zone and fault core, with their plastic or strain-hardening nature, presumably form barriers for the fluid flow, which can compartmentalise the local hydraulic system.

Acknowledgement: Authors thank MOL Hungarian Oil and Gas Company for providing the samples and the financial support of this research. Balázs Kiss (MOL) is thanked for the fruitful discussions on the Mezősas-Furta reservoir.

References

[1] Caine, J.S., Evans, J.P., Forster, C.B., 1996. Fault zone architecture and permeability structure. *Geology* 24, 1025– 1028

[2] Evans, J.P., Forster, C.B., Goddard, J.V., 1997. Permeability of fault-related rocks and implications for fault-zone hydraulic structure. *Journal of Structural Geology* 19, 1393–1404

[3] Ben-Zion, Y., Sammis, C.G.,2003. Characterization of fault zones. *Pure and Applied Geophysics*, 160, 677–715

[4] Tari, G., Dövényi, P., Dunkl, I., Horváth, F., Lenkey, L., Stefanescu, M., Szafián, P., Tóth, T., 1999. Lithospheric structure of the Pannonian basin derived from seismic, gravity and geothermal data. In: Durand B, Jolivet L, Horváth F, Séranne M (eds.): The Mediterranean Basins: Tertiary Extension within the Alpine Orogen. Geological Society, London, Special Publications, 156, p. 215-250

[5] M. Tóth, T., 2008. Repedezett, metamorf fluidumtárolók az Alföld aljzatában. D.Sc. Thesis (In Hungarian)

[6] Balázs, E., Cserepes-Meszéna, B., Nusszer, A., Szili-Gyémánt, P. (1986): An attempt to correlate the metamorphic formations of the Great Hungarian Plain and the Transylvanian Central Mountains (Muntii Apuseni). *Acta Geologica Hungarica*, 29/3-4, 317-320

[7] Szili-Gyémánt, P. (1986): Metamorphic formations in Tiszántúl: The Körös-Berettyó and the Álmosd Units. *Acta Geologica Hungarica*, 29, 305-316

[8] M. Tóth T, Zachar J 2006. Petrology and deformation history of the metamorphic basement in the Mezősas-Furta crystalline high (SE Hungary). *Acta Geol. Hung.*, 49/2, 165-188

[9] Albu, I., A. Pápa 1992: Application of high-resolution seismics in studying reservoir characteristics of hydrocarbon deposits in Hungary. – *Geophysics*, 57/8, pp. 1068–1088

[10] Lőrincz, K.D., 1996. Determination of stress-field history on the basis of multiphase tectonism identified in the seismic profiles, in the western part of the Szolnok flysch belt. *Magyar Geofizika* 37, 228–246 (in Hungarian with English abstract)

[11] Bérubé, D.,Jébrak, M.,1999. High precision boundary fractal analysis for shape characterization. *Computers & Geosciences* 25, 1059–1071

[12] Clark, C.,Mumm, A. S., Collins, A.S., 2006. A coupled micro- and macrostructural approach to the analysis of fluid induced brecciation, Curnamona Province, South Australia, *Journal of Structural Geology* 28, 745–761

[13] Sammis, C.G., Osborne, R.H., Anderson, J.L., Banerdt, M., White, P., 1986. Self-similar cataclasis in the formation of fault gouge. *Pure and Applied Geophysics* 124, 54-77

[14] Sammis, C.G., King, G., Biegel, R., 1987. The kinematics of gouge deformation. *Pure and Applied Geophysics* 125, 777– 812

[15] Blenkinsop, T. G., 1991. Cataclasis and processes of particle size reduction. *Pure and Applied Geophysics* 136, 59– 86

[16] Storti, F., Billi, A., Salvini, F., 2003. Particle size distributions in natural carbonate fault rocks: insights for non-self similar cataclasis. *Earth and Planetary Science Letters* 206, 173–186

[17] Keulen, N., Heilbronner, R., Stünitz, H., Boullier, A.M., Ito, H., 2007. Grain size distribution of fault rocks: A comparison between experimentally and naturally deformed granitoids. *Journal of Structural Geology* 29, 1282-1300

[18] *Mort, K., Woodcock, N.H.*, 2008. Quantifying fault breccia geometry: Dent Fault, NW England. *Journal of Structural Geology* 30, 701-709

[19] Molnár, L., M. Tóth, M., Schubert, F., 2013. Geometric classification of brittle and semi-brittle tectonites in borecore-scale. In: Horváth, J. et al.(eds): Proceedings of V. Congress of Croatian and Hungarian and XVI. Congress of Hungarian Geomathematics, 49-53

[20] Klovan, J. E., Billings, G. K., 1976. Classification of geological samples by discriminant function analysis. *Bulletin of Canadian Petroleum Geology*, 15, 313-330

[21] Davis, J.C., 2002. Statistics and Data Analysis in Geology. Wiley, 638

[22] ISRM, 2006.The complete ISRM suggested methods for rock characterization, testing and monitoring. (Eds: Ulusay, R., Hudson, J. A.) International Society for Rock Mechanics, 628

[23] Cai, M., 2010. Practical estimates of tensile strength and Hoek–Brown strength parameter of brittle rocks. *Rock Mechanics and Rock Engineering* 43/2, 167-184

[24] Martin, C., D., 1993. The strength of massive Lac du Bonnet granite around underground opening. Ph.D. Thesis, 278

[25] Bieniawski, Z.T., 1967. Mechanism of brittle fracture of rock, parts I, II and III. *International Journal of Rock Mechanics and Mining Sciences*, 4, 395–430

[26] Cai, M., Kaiser, P., K., Tasaka,Y., Maejima,T., Morioka, H., Minami, M., 2004. Generalized crack initiation and crack damage stress thresholds of brittle rock masses near underground excavations. *International Journal of Rock Mechanics and Mining Sciences*, 41, 833–847

[27] Hucka, V., Das, B., 1974. Brittleness determination of rocks by different methods. *International Journal of Rock Mechanics and Mining Sciences*, 11, 389–392

[28] Passchier, C.W., Trouw, R. A. J., 2005. Microtectonics, Springer

[29] Hayman, N., W., 2006. Shallow crustal fault rocks from the Black Mountain detachments, Death Valley, CA. *Journal of Structural*

Geology 28, 1767-1784

[30] Aydin, A., 2000. Fractures, faults, and hydrocarbon entrapment, migration and flow. *Marine and Petroleum Geology*, 17, 797-814

[31] Fossen, H., Schultz, R.A., Shipton, Z.K., Mair, K., 2007. Deformation bands in sandstone: a review. *Journal of the Geological Society*, 164

[32] Woodcock, N. H., Dickson, J. A. D., Tarasewicz, J. P. T. 2007. Transient permeability and reseal hardening in fault zones: evidence from dilation breccia textures. In: Lonergan, L., Jolly, R. J. H., Rawnsley, K., Sanderson, D. J. (eds) Fractured Reservoirs. Geological Society, London, Special Publications, 270, 43-53

[33] Storti, F., Balsamo, F., Salvini, F., 2007. Particle shape evolution in natural carbonate granular wear material. *Terra Nova* 19, 344-352.

[34] Caine, J., S., Ronald L. Bruhn, R., L., Forster, C., B., 2010. Internal structure, fault rocks, and inferences regarding deformation, fluid flow, and mineralization in the seismogenic Stillwater normal fault, Dixie Valley, Nevada, *Journal of Structural Geology*, 32, 1576–1589

[35] Matonti, C., Lamarche, J., Guglielmi, Y., Marié, L., 2012: Structural and petrophysical characterization of mixed conduit/seal fault zones in carbonates: Example from the Castellas fault (SE France), *Journal of Structural Geology*, 39, 103-121